IJCEE Vol.10 No.2 December 2024, Page 1-12 ISSN 2598-2931

The 3D Potential Flow Simulation of an Electric Commuter Train's Velocity and Pressure with LISA FEA V.8

Aco Wahyudi Efendi[1]
Email: acowahyudiefendi@student.uns.ac.id

Received : 10 December 2024
Approved : 15 December 2024
Published : 31 December 2024

Abstract: The current research examines the aerodynamic behaviour of an electric commuter rail vehicle moving at 100 km/h by comparing the findings of 3D simulation with manual estimations of dynamic pressure and velocity. Compared to manual approaches, the simulation yielded more accurate insights using the potential flow theory-based LISA FEA V.8 program. There was a 5% discrepancy between the simulation's range of 0.546 kN/m² to 4.865 kN/m² and the manually determined dynamic pressure of 4.633.3 kN/m². The simulation demonstrated the impact of intricate aerodynamic interactions, which produced a velocity of 31.66 m/s, 14% greater than the manual calculation at the train's front of 27.78 m/s.Furthermore, the simulation revealed an uneven velocity distribution contributing to drag, with the highest speeds along the sides and a low-pressure wake at the back. These findings highlight the need for sophisticated simulations to improve train design, lower drag, increase energy efficiency, and improve passenger comfort. They also show the limitations of simplified computations

Keywords: aerodynamic; behavior; lisa; pressure; velocity

[1]Faculty of Engineering, Universitas Sebelas Maret

INTRODUCTION

Urban rail networks, particularly electric commuter trains, are essential to contemporary urban travel. Because these systems run at high speeds, efficiency and safety depend on understanding aerodynamic behaviour, particularly dynamic pressure and velocity. Trains travelling through the air are subject to several influences affecting speed, energy usage, and passenger comfort.

This research examines the dynamic pressure and velocity characteristics of a KRL moving at 100 km/h. It uses a possible fluid flow theory-based 3D simulation with the LISA FEA V.8 program. The aim of this study is to find the dynamic pressure and velocity profiles at various locations on the train's surface, track, and surrounding atmosphere in order to comprehend the aerodynamic consequences.

Aerodynamics is essential for safe and energy-efficient high-speed rail operations. The train's velocity and air pressure interact to produce dynamic forces, which may affect the rail car's structural integrity and stability. Furthermore, variations in dynamic pressure may result in drag, which raises energy consumption. Understanding these forces and velocities is crucial for reducing drag and noise and improving passenger comfort.

The LISA FEA V. 8 software is a valuable tool for simulating possible fluid flows in three dimensions and gaining a thorough understanding of the aerodynamic behavior of high-speed trains. Potential flow theory, by simplifying fluid motion equations, provides a computationally efficient method of analyzing fluid behaviour around the KRL, particularly when the turbulent flow is not present.

The distribution of dynamic pressure along the KRL's surface and the effect of velocity fluctuations on the surrounding fluid flow at a speed of 100 km/h are the two main goals of this study, which uses LISA V.8 FEA. Through an analysis of these variables, the study seeks to pinpoint important

aerodynamic characteristics that influence the train's performance, such as high-pressure zones that could result in drag and locations where variations in velocity could affect stability. The study also aims to shed light on how these fluid dynamic forces affect energy usage and passenger comfort, suggesting improving train design to lower resistance and boost efficiency.

RESEARCH METHOD

Three-dimensional (3D) simulations of possible fluid flow around a KRL at 100 km/h were used in the study. LISA FEA V.8 software, which enables accurate modelling of fluid flow in complex geometries like a train, was used to conduct the simulations. The following are the primary steps in the research method:

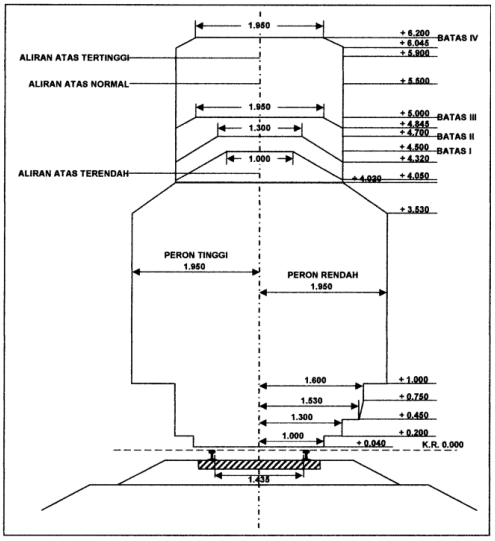

Figure 1. The angle of the railway rails' lying on the bearings

The train body is aluminium alloy and has four easily accessible doors on each side. Its dimensions are 20,000 mm (20 m) in length, 2,800 mm (2.8 m) in width, and 4,145 mm (4.145 m) in height. Its top speeds with a chopper system are 100 km/h (28 m/s), and a VVVF-IGBT system is 110 km/h (31 m/s). With an acceleration rate of 3.3 km/h/s and a standard deceleration rate of 3.7 km/h/s, which can climb to 4.7 km/h/s in emergency conditions, the train has an average weight of 276 tons (276,000 kg). Armature Variable Field (AVF) Chopper Control, Chopper Control-Gate Turn Off (Chopper-GTO), and Variable Voltage Variable Frequency-Insulated Gate Bipolar Transistor (VVVF-IGBT) are all used in the traction system(Atmaja et al., 2019; Bhardawaj et al., 2019; Dash & Majee, 2021; A. W. Efendi, 2023a, 2023b; A. W. Efendi et al., 2022; Esmaeili, M Yousefian, K Nouri, 2019; Etemadi & Saglik, 2021; Fattah et al., 2020; Gharighoran et al., 2018; Hashim, 2020; Koohmishi & Palassi, 2020; Margiantono et al., 2021; Miri et al., 2021; Sayeed & Shahin, 2018; Susanto et al., 2020; Venglár & Lamperová, 2021).

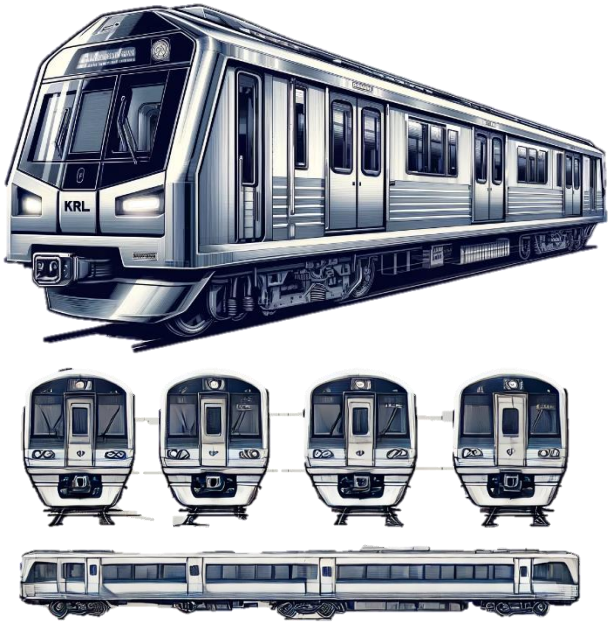

Figure 2. Typical design of KRL

The density of aluminium alloy typically ranges from roughly 25.5 kN/m³ to 27.5 kN/m³. For aluminium alloys, Poisson's ratio shows the connection between axial and lateral strain, which is approximately 0.33. In addition, the modulus of elasticity, which expresses the material's capacity for elastic deformation under stress, is generally in the range of 70,000,000 to 80,000,000 kN/m².

Configuration for Simulation

In the simulation shown in Figure 3, the electric commuter train was modelled in three

dimensions. The train's geometry was produced using intricate CAD models, taking into account all of its main components, including the front nose, body, and undercarriage. To save computing time, the model was slightly simplified while keeping crucial aerodynamic properties.

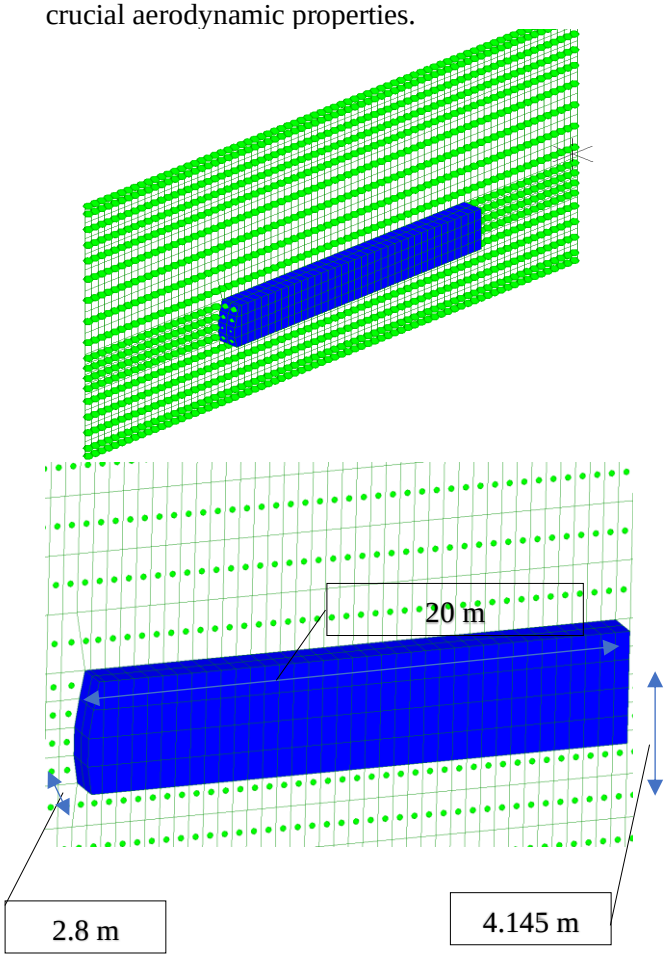

Figure 3. Model of single-vehicle KRL on LISA V.8

The boundary conditions were established according to actual situations in which the train moves through open spaces at a steady speed of 100 km/h. The potential fluid flow method was selected because of its computing efficiency and ability to approximate aerodynamic behaviour accurately without taking into account complex turbulence, which would call for more advanced techniques like computational fluid dynamics (CFD).

Fluid Flow Equations

Potential flow simplifies the Navier-Stokes equations by assuming an irrotational, inviscid fluid. Bernoulli's equation determines the pressure field, while the Laplace equation controls the potential flow, which is solved for velocity potential.

The Laplace equation is satisfied by the velocity potential ϕ:

$$\nabla^2\Phi = 0 \quad (1)$$

From (Φ), the velocity (V) is calculated as the gradient of the potential:

$$V = \nabla\Phi \quad (2)$$

Dynamic pressure (q) is then derived from Bernoulli's equation:

$$q = 1/2\ \rho V^2 \quad (3)$$

Where ρ is the density of air and V is the local velocity.

To compute the potential flow rate of air displaced by a train moving at 100 km/h, we must first figure out the area across which the air flows. The train's width (2.8 m) and height (4.145 m) define the interaction area. The product of these two measurements yields a total size of 11.622 m² (2.8 m multiplied by 4.145 m). It is necessary to translate the train's speed to meters per second, which equals 27.78 m/s (100 km/h divided by 3.6). The following formula can be used to get the potential flow rate: Flow Rate = Area × velocity. By changing the parameters, we can determine that the airflow rate is roughly 323.09 m³/s seen in Figure 4 (Armbruster et al., 2019; Brunskill et al., 2020; C. Y. Li et al., 2020; L. Li et al., 2019; Meng et al., 2019; Sullivan et al., 2020; Zhang et al., 2020).

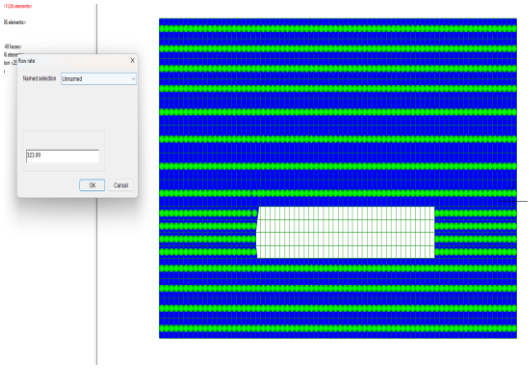

Figure 4. Flow rate zone

The potential flow rate of air around a train travelling at various speeds can be calculated by determining the cross-sectional area of interaction, which is 11.622 m² based on the train's width of 2.8 m and height of 4.145 m. As the speed increases, the flow rate significantly changes: at 25 km/h, the flow rate is approximately 80.73 m³/s; at 50 km/h, it rises to 161.67 m³/s; at 75 km/h, it reaches 242.03 m³/s; and at 100 km/h, it peaks at 323.09 m³/s. These calculations illustrate the substantial volume of air displaced by the train's movement, highlighting the importance of understanding airflow dynamics to enhance aerodynamic efficiency, reduce drag, and improve overall performance in transportation systems.

Table 1. Flow rate value in air based on object velocity

Speed (km/h)	Accelerated (m/s)	Cross-sectional Area (m²)	Flow Rate (m³/s)
25	6.94	11.622	80.73
50	13.89	11.622	161.67
75	20.83	11.622	242.03
100	27.78	11.622	323.09

Mesh Generation

The computational region surrounding the train was discretized using a mesh to address the probable flow issue. The space is divided into small parts via the mesh generation step in LISA FEA V.8, where the potential flow equations are solved iteratively. To capture more precise aerodynamic effects, a coarser mesh was chosen farther away from the train and a finer mesh near the train surface, as shown in Figure 5.

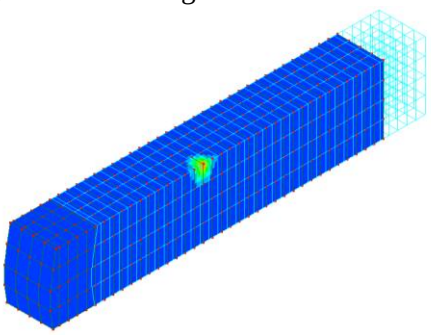

Figure 5. Mesh train modeling Boundary Conditions

The inflow border was adjusted to coincide with the train's 100 km/h speed, or around 27.78 m/s. The outflow barrier was positioned so that, given its distance from the train, it would have the least artificial impact on the outcomes. When necessary, symmetry boundary conditions were used to lessen the computational burden.

Post-Processing

Plotting the velocity and dynamic pressure distributions along the train's surface and the surrounding air allowed for an analysis of the simulation findings. The train's nose, sides, roof, and back were exciting because these sections usually encountered the most significant aerodynamic effects.

Finite element method (FEM)

A mathematical technique called the finite element method (FEM) is used for specific evaluation issues. The restricted component technique combines A few numerical ideas to produce straight or nonlinear framework conditions. Over 20,000 situations are often formed, which is a very high quantity. Therefore, this strategy is not very useful unless a good PC is employed. Strain (distortion), stress, temperature, tension, and stream rate are the outcomes of applying forces on a design, including stress, pressure, temperature stream rate, and severity. The idea behind a body's subsequent movement (twisting) is founded in the

properties of the stress and power structure itself. It is possible to trace the spread of this phenomenon, described as dislodging, in the restricted component.

The finite element technique uses a component discretization method to solve the problem of locating relocations of vertices, associations, grids, and primary powers. Discrete component conditions are associated with the lattice approach for preliminary analysis, and the results are identical to those from traditional structural investigation. Using one-layered components (line components), two-layered components (planar components), or three-layered components (volume/continuum components), discreteness should be possible. This approach uses a continuous component to get a more precise answer (Chatterjee et al., n.d.; A. W. Efendi, 2020; Fadden & McCormick, 2014; Haddad, 2017; G. C. Li et al., 2018; Ngan & Bocher, 2018; Pokkula & Gupta, 2021; Song et al., 2017; Staat et al., 2005; Yin & Shi, 2018).

LISA FEA V.8

LISA FEA V 8. Three distinct types of intensity exchangers had their temperature rise assessed utilizing a well-known restricted component testing tool. The line component, shell, and robust models are arranged in order of simplicity and ease of construction.

For line components, LISA offers a variety of frequently used underlying forms; users need to enter the component's attributes in one exchange box and warm conductivity in a separate dialogue box.

The convection coefficient of the baseplate surface is not established in stone as part of the worth applied elsewhere for line component models solely because research cannot prohibit convection from gathering the baseplate surface using the face determination device. It is only a mental issue.

Incredibly straightforward to stop the flow from the mounting surface for the other two variations; we just do not utilize it. The volume of the entire floor component is regarded as the intensity source for each scenario, and an interior intensity generator is used. Use caution while applying limit conditions to a line component model (Efendi, 2022a, 2022b, 2022c, 2022d, 2023f, 2023d, 2023g, 2023e, 2023c, 2024c, 2024b, 2024a; Efendi & Safitri, 2024; Efendi & Eng, 2024; Sesana et al., 2005).

RESULTS AND DISCUSSION

Dynamic Pressure Distribution

The dynamic pressure distribution on the KRL's surface was found to be non-uniform by the simulation. Since the train's nose is where air first meets the surface, there were the most substantial pressures. The dynamic pressure in this area peaked because of the high relative velocity between the train and the stagnant air. The dynamic pressure falls along the train's sides as the air is displaced and travels parallel to the surface. But again, there was a tiny increase in dynamic pressure near the train's rear, suggesting the establishment of a low-pressure wake zone that generates drag, as seen in Figure 6.

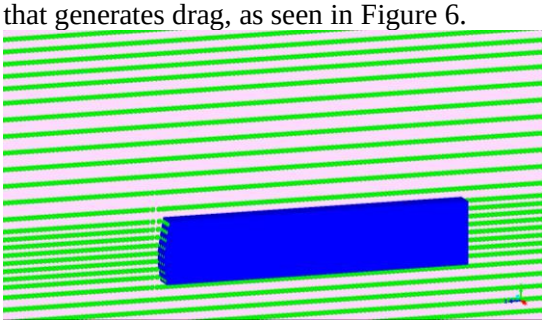

Figure 6. Flow Rate

The air density at ground level is typically around 0.0120 kN/m³, a value essential for various aerodynamics calculations. This density is critical when considering the impact of moving vehicles, such as trains travelling at 100 km/h. Understanding air density is crucial for accurately assessing airflow patterns and forces acting on vehicles. These factors significantly influence design decisions to enhance efficiency and performance in transportation systems, making the knowledge of air density a vital component in engineering applications related to aerodynamics and vehicle dynamics, as seen in Figure 7.

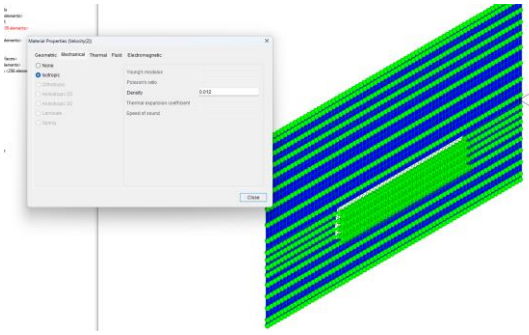

Figure 7. The density of air at ground level

Analyzes the airflow rate that impacts a train car moving at 100 km/h, which comes out to be about 323.5 cubic meters per second. Based on the computed velocity, we estimated the dynamic pressure acting on the train car to be around 4633.3 N/m². The kinetic energy of the air particles hitting the train causes this dynamic pressure. It is important to remember that these estimates are based on an oversimplified model and do not consider intricate details like the aerodynamic form of the train or changes in air density. Dynamic pressure is one of the most important factors in determining the drag force the train experiences.

• Air density (ρ) = 0.012 kN/m³
• Train velocity (V) = 27.78 m/s

Calculating Dynamic Pressure:

• q = 0.5 * 12 kg/m³ * (27.78 m/s)² = 4.6333 kN/m²

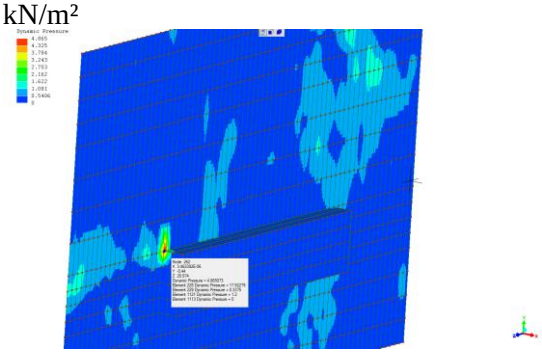

Figure 8. Dynamic pressure

The dynamic pressure determined by the manual computation was 4.6333 kN/m². In the meantime, dynamic pressure values ranging from 0.546 kN/m² to 4.865 kN/m² were obtained from the simulation results using LISA V.8 FEA. When comparing the maximum value from the simulation (4.865 kN/m2) with the manual analysis (4.6333 kN/m2), the ratio of the two values is roughly 1.05. This shows that the manually determined value is 5% lower than the simulated maximum pressure. The disparity between the more sophisticated modelling employed in finite element analysis (FEA) and the assumptions and simplifications made in manual computations can cause this disparity. The variance in the simulation results also draws attention to local pressure variations that can be missed by the manual approach, highlighting the significance of FEA for a more thorough examination of dynamic pressure distribution, as seen in Figure 8.

Speed 25 km/h
Speed 50 km/h
Speed 75 km/h
Speed 100 km/h

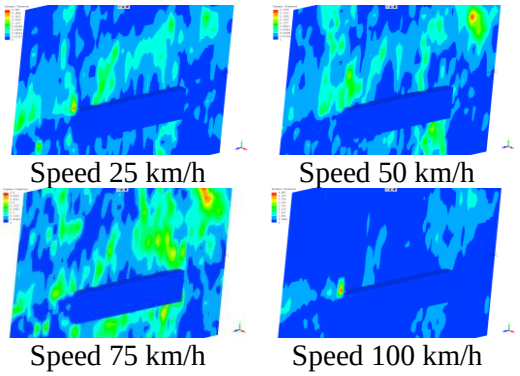

Speed 25 km/h Speed 50 km/h
Speed 75 km/h Speed 100 km/h

Figure 9. Dynamic pressure behaviour at each train speed

Dynamic pressure readings at different speeds (shown in Figure 9 and graph Figure 10) Dynamic pressure is noticeably higher at higher speeds, showing how speed affects pressure. There is a clear relationship between speed and pressure, as the dynamic pressure value drops significantly with speed. Higher speeds usually result in a more significant pressure drop, but there is variation in the amount of pressure drop at certain speed intervals. This illustrates how the quadratic character of the dynamic pressure formula results in a nonlinear relationship between pressure and velocity. These data emphasize how important velocity control is for controlling dynamic forces in engineering applications.

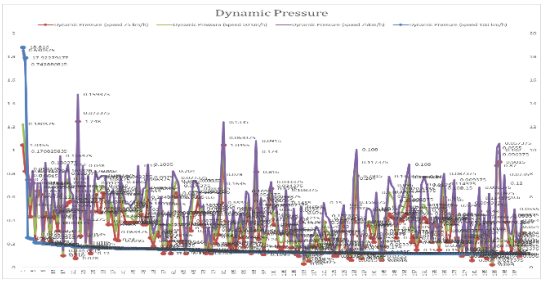

Figure 10. Dynamic pressure graph at each train speed

Velocity Distribution

According to this, the velocity distribution was not uniform. The highest velocities were recorded on the train's flanks, where the air flows gently. These patches, which had velocities marginally higher than the train's speed, showed the acceleration of air particles surrounding the train's body.

The simulation showed that the wake creation caused a significant decline in velocity near the back of the train. The additional drag caused by the low-velocity wake may affect the train's overall efficiency. This result emphasizes how crucial aerodynamic design is in the back of the train to minimize drag and wake production.

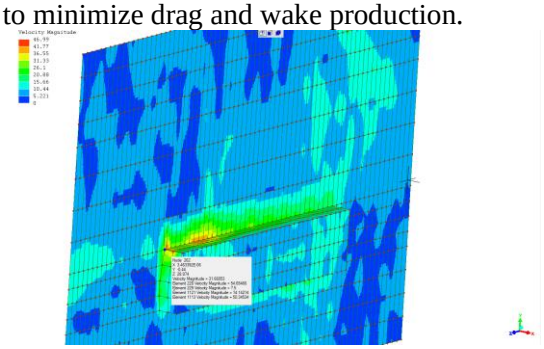

Figure 11. Velocity distribution

The KRL's velocity, as calculated manually, was 27.78 m/s (Table 1 assuming a KRL speed of 100 km/h). However, a dynamic pressure with velocities ranging from 5.221 m/s to 46.99 kN/m² was obtained from the simulation using LISA V.8 FEA, with a velocity of 31.66 m/s recorded at the front of the KRL. The ratio is roughly 1.14 when comparing the simulation's velocity of 31.66 m/s to the manual analysis result of 27.78 m/s. This suggests that perhaps as a result of localized effects and aerodynamic considerations in the simulation, the simulated velocity is 14% greater than the manually determined velocity, as seen in Figure 11.

Speed 25 km/h
Speed 50 km/h
Speed 75 km/h
Speed 100 km/h

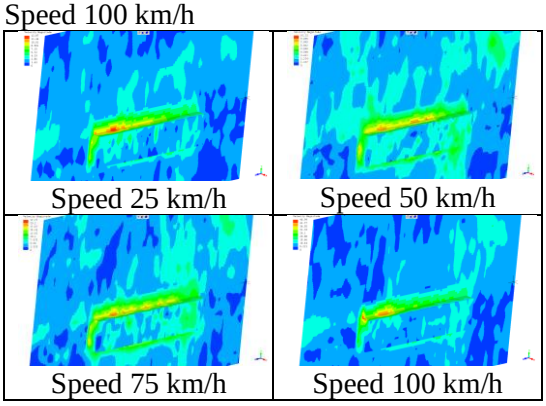

Figure 12. Velocity distribution behavior at each train speed

The velocity magnitude begins at a higher value of 56 for a 100 km/h speed and steadily drops to about 14.15. A similar pattern is shown for 75 km/h, with the velocity magnitude starting at 14.42 and gradually declining to about 8.5. The velocity magnitude starts at about 6.4 and tapers off to about 4.06 when the speed drops to 50 km/h. Finally, the velocity magnitude decreases even further at 25 km/h, falling from about 11.13 to 4.

Given that speed and velocity magnitude have an inverse connection, the general trend shows that the velocity magnitude decreases proportionately as speed decreases, as shown in Figure 12 and Graph Figure 13.

Figure 13. Velocity distribution graph at each train speed

CONCLUSION

The analysis of the velocity distribution and dynamic pressure on a KRL moving at 100 km/h provides crucial information about the aerodynamic performance of high-speed trains. The results of the 3D potential flow simulation using LISA FEA V.8 identified the important places where pressure and velocity fluctuations are most significant.

The KRL (Commuter Line) train's surface has a non-uniform dynamic pressure distribution, with the maximum pressure at the train's nose because of the high relative

velocity between the train and the stagnant air. The dynamic pressure drops as the air passes along the train's sides, but it slightly rises close to the back, suggesting the creation of a low-pressure wake zone that adds to drag. Ground-level air density, usually about 0.012 kN/m³, performs a significant role in aerodynamic calculations by affecting airflow patterns and the forces exerted on moving objects, such as trains. It is essential to comprehend these factors in order to maximize the performance and design of transportation networks.

Considering simplified models, the dynamic pressure was calculated to be 4633.3 N/m² while examining the airflow rate surrounding a train travelling at 100 km/h. However, dynamic pressures ranging from 0.546 to 4.865 kN/m² were revealed by simulations using LISA V.8 FEA. The limits of simplified manual calculations in comparison to more complicated finite element analysis (FEA) are shown by the 5% discrepancy between the manually calculated value and the maximum pressure in the simulation. Considering local pressure differences, the simulations offer a more accurate picture, highlighting the importance of sophisticated modelling for in-depth aerodynamic investigation.

Furthermore, there is an uneven velocity distribution around the train, with the maximum velocities found close to the sides where air flows more quickly and a steep velocity drop in the back because of the wake. The train's efficiency is decreased by this wake, which also increases drag. Further illustrating the influence of aerodynamic elements not adequately represented in simplified models, the simulation recorded a train velocity of 31.66 m/s at the nose, which was 14% higher than the manually computed 27.78 m/s. As speed is decreased, the velocity magnitude reduces proportionately, highlighting the significance of aerodynamic design in reducing drag and enhancing overall performance at different speeds.

REFERENCES

Armbruster, W., Hardi, J. S., Suslov, D., & ... (2019). Injector-driven flame dynamics in a high-pressure multi-element oxygen-hydrogen rocket thrust chamber. Journal of Propulsion and …. https://doi.org/10.2514/1.B37406

Atmaja, D. S., Aghastya, A., Bramasta, A. R., & ... (2019). Designing Track Holder Device for Maintaining Spoor Width In Railway Geometry Maintenance. Journal of Physics …. https://doi.org/10.1088/1742-6596/1273/1/012064

Bhardawaj, S., Sharma, R. C., & ... (2019). A Survey of Railway Track Modelling. International Journal of …. http://search.ebscohost.com/login.aspx?direct=true%5C&profile=ehost%5C&scope=site%5C&authtype=crawler%5C&jrnl=09753060%5C&AN=142586177%5C&h=LUdVoNYv%2BvACUj7aTi1qq4jdRk57JI7Ovt1O%2FqE%2BEQfnjjZEG7n6WTTKgUGdrDbSHimUUt53WeFNnPRAOHHhuA%3D%3D%5C&crl=c

Brunskill, H., Hunter, A., Zhou, L., & ... (2020). An evaluation of ultrasonic arrays for the static and dynamic measurement of wheel-rail contact pressure and area. …, Part J: Journal of …. https://doi.org/10.1177/1350650120919889

Chatterjee, A. K., Bhowmick, A., & Bagchi, A. (n.d.). Finite Element Modeling and Analysis of Light-gauge Steel Plate Shear Walls.

Dash, S. K., & Majee, A. (2021). Geogrid Reinforcement for Stiffness Improvement of Railway Track Formation Over Clay Subgrade. International Journal of Geomechanics. https://doi.org/10.1061/(ASCE)GM.1943-5622.0002128

Efendi, A. W. (2020). Modeling of soil subsidence in IKN using numerical analysis of the finite element method LISA V. 8. Researchgate. Net. https://www.researchgate.net/profile/Aco-Efendi/publication/367090313_Modeling_of_soil_subsidence_in_IKN_using_numerical_analysis_of_the_finite_element_method_LISA_V8/links/63c0f9964c7e

7c4e5125262a/Modeling-of-soil-subsidence-in-IKN-using-numerical-analysis-of-the-finite-element-method-LISA-V8.pdf

Efendi, A. W. (2022a). Behavior Analysis of Building Structures After a Fire with FEA LISA V. 8. Kurva S: Jurnal Keilmuan Dan Aplikasi Teknik …. http://ejurnal.untag-smd.ac.id/index.php/TEKNIKD/article/view/6413

Efendi, A. W. (2022b). Repair analysis of Pinang Bridge oprit subsidence with mortar form using LISA FEA. Journal of Research and Innovation in Civil …. https://jurnal.politap.ac.id/index.php/rigid/article/view/1193

Efendi, A. W. (2022c). Structural Design Tuak River Pedestrian Suspension Bridge Anchor Block Type Rigid Symmetric with LISA. Elektriese: Jurnal Sains Dan Teknologi Elektro. https://jurnal.itscience.org/index.php/elektriese/article/view/1572

Efendi, A. W. (2022d). Structural Design Tuak River Pedestrian Suspension Bridge Anchor Block Type Rigid Symmetric with LISA. Elektriese: Jurnal Sains Dan Teknologi Elektro. https://jurnal.itscience.org/index.php/elektriese/article/view/1572

Efendi, A. W. (2023a). Behavior of Railroad Bridge Girders Due to Brake Loads with LISA V. 8 FEA. … Conference on Railway and Transportation (ICORT …. https://www.atlantis-press.com/proceedings/icort-22/125985594

Efendi, A. W. (2023b). Behavior of Railroad Bridge Girders Due to Brake Loads with LISA V. 8 FEA. … Conference on Railway and Transportation (ICORT …. https://www.atlantis-press.com/proceedings/icort-22/125985594

Efendi, A. W. (2023c). Pemodelan penurunan tanah di ibu kota negara nusantara menggunakan analisis numerik metode elemen hingga lisa v. 8. PADURAKSA: Jurnal Teknik Sipil …. https://www.ejournal.warmadewa.ac.id/index.php/paduraksa/article/view/5643

Efendi, A. W. (2023d). Simulation of fire exposure behavior to building structural elements using LISA FEA V. 8. International Journal of Advanced Science and …. http://www.ijasca.org/index.php/ijasca/article/view/31

Efendi, A. W. (2023e). Stress Behavior of Rampdoor Jetty Bumi Harapan Port Sepaku-IKN Using LISA FEA V. 8. Jurnal Rekayasa Mesin Dan Inovasi Teknologi …. https://www.researchgate.net/profile/Aco-Efendi/publication/378555312_Stress_Behavior_of_Rampdoor_Jetty_Bumi_Harapan_Port_Sepaku-IKN_Using_LISA_FEA_V8/links/65e019dcadf2362b635ccf97/Stress-Behavior-of-Rampdoor-Jetty-Bumi-Harapan-Port-Sepaku-IKN-Using-LISA-FEA-V8.pdf

Efendi, A. W. (2023f). The Settlement Behavior Using Replacement Embankment with Mortar Foam and Geofoam using LISA FEA. Nusantara Civil Engineering Journal. http://ojs.poltekba.ac.id/ojs/index.php/nuce/article/view/484

Efendi, A. W. (2023g). The Settlement Behavior Using Replacement Embankment with Mortar Foam and Geofoam using LISA FEA. Nusantara Civil Engineering Journal. http://ojs.poltekba.ac.id/ojs/index.php/nuce/article/view/484

Efendi, A. W. (2024a). APPLICATION OF CHATGPT IN THE ANALYSIS OF INTERNAL FORCES OCCURRING IN SIMPLE BEAMS USING LISA V. 8 FEA. Selodang Mayang: Jurnal Ilmiah Badan …. https://ojs.selodangmayang.com/index.php/bappeda/article/view/313

Efendi, A. W. (2024b). Behavior of welded joints on the roof truss of KOJK Office using LISA V. 8 FEA. Journal of Metallurgical Engineering and Processing ….

http://jurnal.upnyk.ac.id/index.php/jmept/article/view/12020

Efendi, A. W. (2024c). Characteristic behavior of soil using bacterial biogrouting with LISA FEA V. 8. International Journal of Advanced Science and …. http://ijasca.org/index.php/ijasca/article/view/47

Efendi, A. W., & Safitri, N. (2024). Behavior of Cakar Ayam Modifikasi (CAM) foundation on soft soil with LISA V. 8 FEA. Kurva S: Jurnal Keilmuan Dan Aplikasi …. https://www.researchgate.net/profile/Aco-Efendi/publication/381226408_Behavior_of_Cakar_Ayam_Modifikasi_CAM_foundation_on_soft_soil_with_LISA_V8_FEA/links/6662669285a4ee7261ab122a/Behavior-of-Cakar-Ayam-Modifikasi-CAM-foundation-on-soft-soil-with-LISA-V8-FEA.pdf

Efendi, A. W., Zulkarnain, A., & Atmaja, D. S. (2022). Behavior of railroad bearing due to temperature and load using LISA FEA. Journal of Railway Transportation …. https://mail.jrtt.org/jrtt/article/view/1

Efendi, I. A. W., & Eng, A. (2024). Structural Performance and Stress Contour Analysis of Multi Utility Tunnels Using LISA V. 8 Finite Element Analysis. Journal of Research and Innovation in Civil …. https://jurnal.politap.ac.id/index.php/rigid/article/view/1589

Esmaeili, M Yousefian, K Nouri, R. (2019). Vertical load distribution in ballasted railway tracks with steel slag and limestone ballasts. IJTI International Journal of Transportation and …international Journal of …. https://doi.org/10.1080/10298436.2017.1380808

Etemadi, A., & Saglik, H. (2021). Fatigue Assessment of Welded Connections in I-Girder Composite High-Speed Railway Bridges. Journal of Bridge Engineering. https://doi.org/10.1061/%28ASCE%29BE.1943-5592.0001685

Fadden, M., & McCormick, J. (2014). Finite element model of the cyclic bending behavior of hollow structural sections. Journal of Constructional Steel Research. https://www.sciencedirect.com/science/article/pii/S0143974X13003040

Fattah, M. Y., Al-Qaissi, M. R. M., & Aswad, M. F. (2020). Settlement of railway track on reinforced ballast overlain by clayey. Journal of Transportation …. https://dergipark.org.tr/en/pub/jtl/issue/57872/829091

Gharighoran, A., Heydari-Noghabi, H., & Moeini, A. (2018). Numerical Investigation of HMA Effect on Dynamic Behaviour of Railway Track Transition Zone. Journal of Structural and …. https://www.jsce.ir/article_48106.html?lang=en

Haddad, M. (2017). Cyclic behavior and finite element modeling of wide flange steel bracing members. Thin-Walled Structures. https://www.sciencedirect.com/science/article/pii/S0263823116308333

Hashim, A. S. (2020). Motion Sensors for Speed in Railway Engineering. Journal of Electrical Power and Electronic Systems. http://fazpublishing.com/jepes/index.php/jepes/article/view/33

Koohmishi, M., & Palassi, M. (2020). Degradation of railway ballast under compressive loads considering particles rearrangement. … Journal of Pavement Engineering. https://doi.org/10.1080/10298436.2018.1449949

Li, C. Y., Tim, K. T., & Hu, G. (2020). Dynamic mode decomposition on pressure flow field analysis: Flow field reconstruction, accuracy, and practical significance. Journal of Wind Engineering and Industrial …. https://www.sciencedirect.com/science/article/pii/S0167610520301884

Li, G. C., Tian, F., Yang, Z. J., & Zhang, G. Z. (2018). Finite Element Analysis on K-Type External Braced Steel Frame System. Key Engineering Materials. https://www.scientific.net/KEM.763.495

Li, L., Peng, G., Wang, J., Gong, J., & Meng,

S. (2019). Numerical and experimental study on keyhole and melt flow dynamics during laser welding of aluminium alloys under subatmospheric pressures. International Journal of Heat and …. https://www.sciencedirect.com/science/article/pii/S0017931018343382

Margiantono, A., Setijo, H., & ... (2021). Railway Vibration Level in Semarang City. Journal of Physics …. https://doi.org/10.1088/1742-6596/1825/1/012102

Meng, M., Zamanipour, Z., Miska, S., Yu, M., & ... (2019). Dynamic stress distribution around the wellbore influenced by surge/swab pressure. Journal of Petroleum …. https://www.sciencedirect.com/science/article/pii/S0920410518307721

Miri, A., Thambiratnam, D. P., & Chan, T. (2021). Thermal challenges of replacing jointed rails with CWR on steel railway bridges. Journal of Constructional Steel …. https://www.sciencedirect.com/science/article/pii/S0143974X21001085

Ngan, N. H., & Bocher, P. (2018). Finite element analysis simulation of the effect of induction hardening on rolling contact fatigue. Journal of Tribology. https://asmedigitalcollection.asme.org/tribology/article-abstract/140/6/061404/383814

Pokkula, R., & Gupta, T. V. K. (2021). Finite Element Method Based Evaluation of Bogie Bolster Design. … Journal of Vehicle Structures \& …. http://search.ebscohost.com/login.aspx?direct=true%5C&profile=ehost%5C&scope=site%5C&authtype=crawler%5C&jrnl=09753060%5C&AN=151614565%5C&h=timGZXkT3zcplpAJAQbZ6pIJm%2BdlACKfpIYj8oAJBFXrTBhfcoTi4W9o9%2FRcDeTBnd9xuns4Zo2DsqoTJu0R8g%3D%3D%5C&crl=c

Sayeed, M. A., & Shahin, M. A. (2018). Design of ballasted railway track foundations using numerical modelling. Part I: Development. Canadian Geotechnical Journal. https://doi.org/10.1139/cgj-2016-0633

Sesana, A., Haardt, F., Madau, P., & ... (2005). The gravitational wave signal from massive black hole binaries and its contribution to the LISA data stream. … Astrophysical Journal. https://doi.org/10.1086/428492

Song, T., Liu, Y., & Wang, Y. (2017). Finite Element Method for Modeling 3D Resistivity Sounding on Anisotropic Geoelectric Media. Mathematical Problems in Engineering, 2017, 1–12. https://doi.org/10.1155/2017/8027616

Staat, M., Heitzer, M., Lang, H., & Wirtz, K. (2005). Direct finite element route for design-by-analysis of pressure components. … Journal of Pressure Vessels and Piping. https://www.sciencedirect.com/science/article/pii/S0308016104001073

Sullivan, R., Kok, J. F., Katra, I., & ... (2020). A broad continuum of aeolian impact ripple morphologies on Mars is enabled by low wind dynamic pressures. Journal of Geophysical …. https://doi.org/10.1029/2020JE006485

Susanto, A., Artono, B., Khonjun, S., & ... (2020). Denoising of disturbed signal using reconstruction technique of emd for railway bearing condition monitoring. International Journal of …. https://www.academia.edu/download/65473215/PaperdariIJCSI_Denoising_of_Disturbed_Signal_using_Reconstruction.pdf

Venglár, M., & Lamperová, K. (2021). Effect of the Temperature on the Modal Properties of a Steel Railroad Bridge. Slovak Journal of Civil Engineering. https://search.proquest.com/openview/90e6a8e5513683ea693640acb773cf90/1?pq-origsite=gscholar%5C&cbl=2026652

Yin, H., & Shi, G. (2018). Finite element analysis on the seismic behavior of fully prefabricated steel frames. Engineering Structures. https://www.sciencedirect.com/science/article/pii/S0141029618302645

Zhang, Q., Qian, X., Chen, Y., & Yuan, M. (2020). Deflagration shock wave

dynamics of DME/LPG blended clean fuel under the coupling effect of initial pressure and equivalence ratio in elongated closed space. Journal of Cleaner Production. https://www.sciencedirect.com/science/article/pii/S0959652619344427